AMERICAN SOCIETY FOR MICROBIOLOGY | Molecular and Cellular Biology®

RESEARCH ARTICLE

E2F-2 Promotes Nuclear Condensation and Enucleation of Terminally Differentiated Erythroblasts

Kelsey L. Swartz,[a,b] Scott N. Wood,[c] Tushar Murthy,[a,b] Oscar Ramirez,[d] Gangjian Qin,[e] Manoj M. Pillai,[d] Sridhar Rao,[c,f,g] Alex C. Minella[c,f,h]

Department of Medicine, Division of Hematology/Oncology,[a] Driskill Graduate Program in Life Sciences,[b] and Feinberg Cardiovascular Research Institute,[e] Northwestern University Feinberg School of Medicine, Chicago, Illinois, USA; Blood Research Institute, BloodCenter of Wisconsin, Milwaukee, Wisconsin, USA[c]; Section of Hematology, Yale Cancer Center, New Haven, Connecticut, USA[d]; Department of Cell Biology, Neurobiology, and Anatomy,[f] Department of Pediatrics,[g] and Department of Medicine,[h] Medical College of Wisconsin, Milwaukee, Wisconsin, USA

ABSTRACT E2F-2 is a retinoblastoma (Rb)-regulated transcription factor induced during terminal erythroid maturation. Cyclin E-mediated Rb hyperphosphorylation induces E2F transcriptional activator functions. We previously reported that deregulated cyclin E activity causes defective terminal maturation of nucleated erythroblasts *in vivo*. Here, we found that these defects are normalized by E2F-2 deletion; however, anemia in mice with deregulated cyclin E is not improved by E2F-2-loss, which itself causes reduced peripheral red blood cell (RBC) counts without altering relative abundances of erythroblast subpopulations. To determine how E2F-2 regulates RBC production, we comprehensively studied erythropoiesis using knockout mice and hematopoietic progenitors. We found that efficient stress erythropoiesis *in vivo* requires E2F-2, and we also identified an unappreciated role for E2F-2 in erythroblast enucleation. In particular, E2F-2 deletion impairs nuclear condensation, a morphological feature of maturing erythroblasts. Transcriptome profiling of E2F-2-null, mature erythroblasts demonstrated widespread changes in gene expression. Notably, we identified citron Rho-interacting kinase (CRIK), which has known functions in mitosis and cytokinesis, as induced in erythroblasts in an E2F-2-dependent manner, and we found that CRIK activity promotes efficient erythroblast enucleation and nuclear condensation. Together, our data reveal novel, lineage-specific functions for E2F-2 and suggest that some mitotic kinases have specialized roles supporting enucleation of maturing erythroblasts.

KEYWORDS E2F, cell cycle, cell differentiation, enucleation, erythropoiesis, gene regulation, mouse models

Received 12 May 2016 **Returned for modification** 12 June 2016 **Accepted** 4 October 2016

Accepted manuscript posted online 17 October 2016

Citation Swartz KL, Wood SN, Murthy T, Ramirez O, Qin G, Pillai MM, Rao S, Minella AC. 2017. E2F-2 promotes nuclear condensation and enucleation of terminally differentiated erythroblasts. Mol Cell Biol 37:e00274-16. https://doi.org/10.1128/MCB.00274-16.

Address correspondence to Alex C. Minella, alex.minella@bcw.edu.

In maturing erythroid progenitors, control of cell cycle progression is intrinsically linked to their morphological and functional maturation programs. For one, during the transition from CFU-erythroid (CFU-E) progenitors to proerythroblasts, S-phase progression is required for chromatin changes that promote the induction of differentiation stage-specific genes (1). Erythroblasts exit the mitotic cell cycle before undergoing enucleation; this exit occurs concomitantly with the induction of cyclin-dependent kinase (Cdk) inhibitors, including $p21^{Cip1}$ and $p27^{Kip1}$ (2–4). Loss of retinoblastoma (Rb), the master regulator of G_1-to-S-phase progression, results in ineffective erythropoiesis *in vivo* (5–8). Upstream mitogen-stimulated pathway signaling converges upon the G_1 cyclin-Cdks, leading to Rb hyperphosphorylation and E2F transcription factor activation (9–11). Deregulation of cyclin E-Cdk2 activity, caused by disruption of the major pathway that controls ubiquitin-mediated destruction of cat-

alytically active cyclin E, induces dyserythropoiesis associated with cell-autonomous effects on survival and gene expression (12–14).

A number of studies have focused on understanding physiologic functions of both Rb-regulated and Rb-independent E2F transcription factors in erythroid cells, and these studies have focused primarily on their roles in regulating progenitor proliferation. Two Rb-regulated E2F transcriptional activators, E2F-1 and E2F-2, cooperate in the generation of erythroid cell precursors *in vivo* (15). In terminally differentiated erythroid cells, E2F-2 is directly regulated by Krüppel-like factor 1 (EKLF), a lineage-specific transcription factor. EKLF loss results in aberrant S-phase entry due to *E2f2* gene misregulation (16, 17). Both E2F-2 and one of its binding partners, Dp-2, are induced during erythroid differentiation, and Dp-2 loss results in macrocytic erythrocytes and accumulation of terminally differentiating erythroid cells in S phase (18). Germ line deletion of another E2F transcription factor, E2F-4, results in fetal anemia due to impaired expansion (19, 20). One of the Rb-independent E2F family members, E2F-8, collaborates with Rb to restrain E2F-2 transcriptional activity during erythroid maturation and prevent DNA damage, permitting normal red blood cell (RBC) production (7). Moreover, E2F-2 loss alleviates erythroid differentiation defects seen with Rb loss alone or in combination with deletion of *E2f8* (7, 8).

Complete loss of E2F-2, the dominantly expressed Rb-regulated E2F in terminally differentiated erythroblasts, causes anemia in mice (15); however, the mechanisms by which E2F-2 controls RBC production are incompletely defined. Here, we show that E2F-2 has key functions in both stress and steady-state erythropoiesis. During stress, E2F-2 is required for normal S-phase progression and expansion of the splenic erythroid compartment. By studying steady-state erythropoiesis, we found that E2F-2 regulates enucleation of mature erythroblasts, and we further identified a role for E2F-2 in promoting nuclear condensation in late-stage erythroblasts. RNA sequencing reveals widespread defects in gene expression in primary, *E2f2*-null erythroblasts, indicating an extensive E2F-2-dependent gene expression program during terminal maturation. One gene demonstrating E2F-2-dependent induction in differentiated erythroid cells is *Cit*, encoding citron Rho-interacting kinase (CRIK), a mitotic kinase whose activity we found promotes nuclear condensation and enucleation in terminally differentiated erythroid cells. Our results demonstrate a multifaceted role for E2F-2 during erythropoiesis and illuminate important functions for E2F-2 in the control of erythroblast enucleation.

RESULTS

Bone marrow erythroid cell maturation defects associated with deregulated cyclin E-Cdk2 activity are E2F-2 dependent. Previously, gene expression studies have demonstrated that, of all E2F transcription factor genes, *E2f2* is most significantly induced in terminally differentiating cells of the definitive erythroid lineage (in bone marrow and fetal liver) (7, 21). In agreement with these gene expression data, we found that E2F-2 protein is significantly upregulated in primary bone marrow erythroid cells, sorted based on CD44/Ter119/forward scatter (FSC) (22) to distinguish basophilic erythroblasts (RII), polychromatic erythroblasts (RIII), and orthochromatic erythroblasts (RIV) (Fig. 1A and C). We further compared protein expression of Rb-regulated E2F-1, -2, -3, and -4 during *in vitro* erythroid differentiation of primary hematopoietic progenitors obtained from wild-type fetal livers, an experimental system that is well suited for studying terminal erythroid cell maturation (23). We found that only E2F-2 is induced upon erythroid differentiation and that it remains elevated throughout maturation (Fig. 1B). These data are consistent with results from a prior study of E2F protein expression assayed directly from sorted fetal liver erythroid cell subpopulations (8).

Rb hyperphosphorylation, mediated by cyclin E-Cdk2 complexes, promotes E2F-dependent transcriptional activity (24, 25). We have previously reported the generation of a cyclin $E^{T74A\ T393A}$ knock-in mouse model, in which the major ubiquitylation pathway (controlled by SCF^{Fbw7}) for catalytically active cyclin E is disabled by mutations in its Cdc4 phosphodegron motifs (12). In this model, hyperstable cyclin E results in defective terminal erythroid maturation, with abnormal accumulation of basophilic

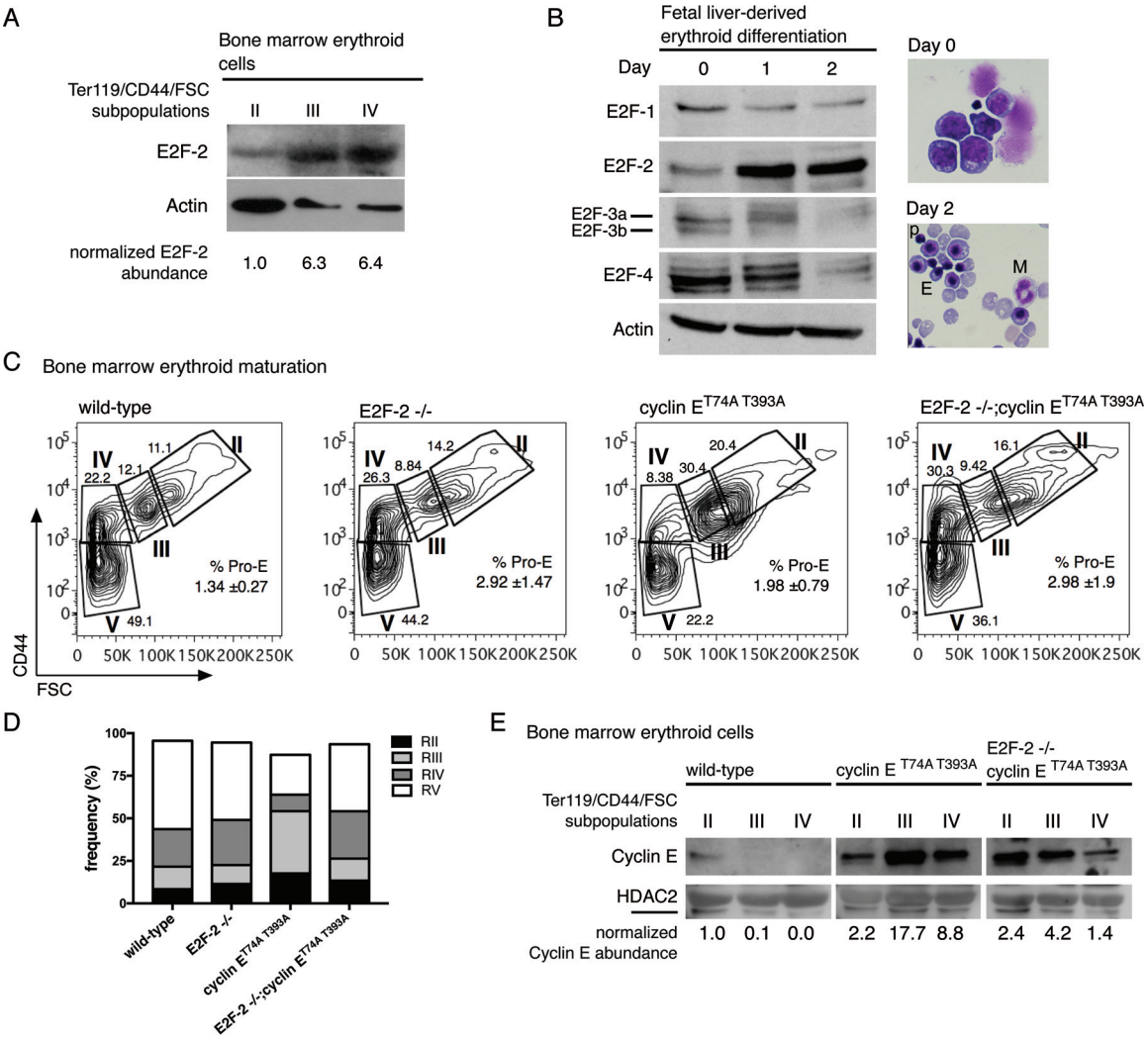

FIG 1 Bone marrow erythroid cell maturation defects associated with deregulated cyclin E-Cdk2 activity are E2F-2 dependent. (A) Ter119-positive bone marrow cells were sorted by expression of CD44 versus FSC (gating as shown in panel C) and collected for immunoblot analysis; relative abundance of E2F-2 compared to loading control is indicated. (B) Hematopoietic progenitors obtained from wild-type fetal livers were differentiated to the erythroid lineage in culture as shown (right panels). Left, cells were harvested at the indicated time points and immunoblotted for E2F transcription factors, with β-actin shown as a loading control. Right, representative micrographs (magnification, $\times$100) of fetal liver progenitors (top) and cells obtained after 2 days in erythroid differentiation culture (bottom), in which the dominant morphologies are mature, nucleated erythroid cells (E, orthochromatic erythroblast form) and enucleated erythroid cells. p, pyrenocyte; M, mature myeloid cell (neutrophil). (C) Erythroid maturation was studied using Ter119$^+$ bone marrow cells collected from age- and sex-matched mice of the indicated genotypes, and representative CD44/FSC plots are shown with the percentage of cells in each subpopulation labeled. The frequency of proerythroblasts, gated based on CD44^{high} Ter119^{dim}, is shown as mean values with corresponding standard deviations derived from 4 to 8 mice of each genotype. (D) Percentages of cells in each erythroid subpopulation region (RII to RV) shown in panel C, representing averages from 4 to 8 mice per genotype. *P* values for cyclin E$^{T74A\ T393A}$ versus E2F-2$^{-/-}$; cyclin E$^{T74A\ T393A}$ comparison: RII, 0.26; RIII, 0.001; RIV, $\leq$0.0001. Comparisons between relative abundances of erythroid subpopulations revealed no statistically significant differences between wild-type and E2F-2 knockout mice or between wild-type and E2F-2$^{-/-}$; cyclin E$^{T74A\ T393A}$ mice (*P* values for the latter comparison: RII, 0.56; RIII, 0.95; RIV, 0.69). (E) The indicated bone marrow erythroid subpopulations from the specified genotypes were sorted as shown in panel C, and lysates were prepared and immunoblotted. Samples were electrophoresed and blotted together using two gels and membranes imaged simultaneously. A representative immunoblot demonstrating cyclin E protein expression and HDAC2 as a nucleoprotein used for normalization is shown from three separate experiments, with relative abundance measurements indicated.

erythroblasts, reduced numbers of orthochromatic erythroblasts and reticulocytes, and anemia (12, 13). Because cyclin E knock-in erythroid cells exhibit hyperphosphorylated Rb (13) and E2F-2 is the major E2F transcriptional activator expressed in late-stage bone marrow erythroid cells, we hypothesized that E2F-2 deletion would revert the defective maturation phenotypes found in cyclin E knock-in bone marrows. To test this, we crossed cyclin E$^{T74A\ T393A}$ mice with E2F-2 knockout mice and studied erythroid maturation in resulting animals. Consistent with our hypothesis, deletion of E2F-2 in the

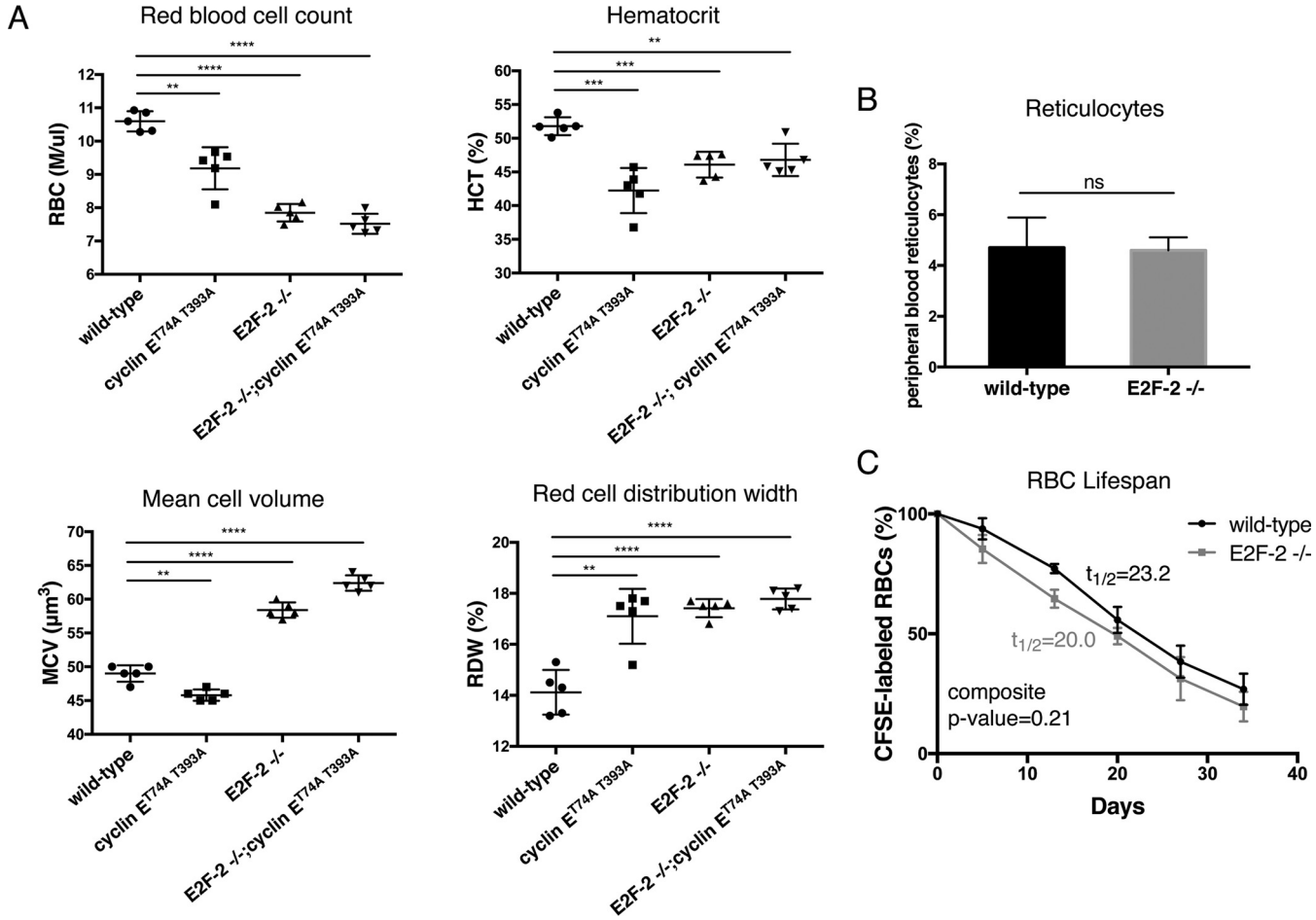

FIG 2 RBC abnormalities associated with E2F-2 deletion *in vivo*. (A) Red cell parameters from peripheral blood of age- and sex-matched mice in the indicated genotypes. Each symbol represents an individual mouse. ****, $P \leq 0.0001$; ***, $P \leq 0.001$; **, $P \leq 0.01$. (B) Peripheral blood from wild-type and E2F-2-null age- and sex-matched mice was collected, stained with thiazole orange, and analyzed by flow cytometry. Data are shown as the percentage of reticulocytes and are derived from 5 mice per genotype. Error bars represent standard deviations; $P = 0.85$. (C) RBCs were isolated from the peripheral blood of wild-type and E2F-2-null mice, stained with CFSE, and injected into wild-type recipient animals. Peripheral blood was collected from recipient animals at the indicated time points, and the frequency of labeled cells remaining was determined by flow cytometry. Half-lives were calculated using the slope of the trend line. The graph shows results of a representative experiment using four animals of each genotype; the composite *P* value was calculated from 3 separate experiments.

setting of cyclin E$^{T74A\ T393A}$ expression restored the normal relative abundances of bone marrow erythroblast subpopulations (Fig. 1C and D). Because expression of cyclin E itself is positively regulated by E2F transcriptional activity (26), we considered the possibility that cyclin E$^{T74A\ T393A}$ synthesis in E2F-2-null erythroblasts could be reduced to the extent that the phosphodegron mutations exert a negligible impact upon cyclin E abundance. We found that E2F-2-loss partially mitigates accumulation of the Fbw7-resistent cyclin E protein; however, immunoblot assays of sorted erythroblast subpopulations revealed a marked increase of cyclin E$^{T74A\ T393A}$ protein in both *E2f2* wild-type and null settings compared to wild-type cyclin E in control erythroblasts (Fig. 1E). In summary, while the positive feedback loop connecting E2F and cyclin E-Cdk2 activities may contribute to our observation of epistasis in the erythroid lineage with the cyclin E knock-in, E2F-2 knockout crosses, our data indicate that E2F-2 is a key mediator of phenotypes associated with deregulated cyclin E activity in terminally differentiated erythroid cells.

Anemia associated with deregulated cyclin E-Cdk2 *in vivo* is not rescued by E2F-2 deletion. Though E2F-2 deletion reverts deregulated cyclin E-associated erythroblast maturation defects in bone marrow resolvable by immunophenotyping, compound mutant mice remain anemic (Fig. 2A). E2F-2 knockout mice themselves are known to be anemic (15), despite demonstrating immunophenotypically normal bone

marrow erythroblast subpopulations (Fig. 1C), with reduced red blood cell counts, larger mean cell volumes, and increased red cell distribution width (Fig. 2A). E2F-2-knockout, cyclin $E^{T74A\ T393A}$ mice exhibited similar red blood cell (RBC) parameters (Fig. 2A). These data indicate that E2F-2 activity is required to maintain normal RBC counts, irrespective of cyclin E-Cdk2 activity regulation.

E2F-2 knockout mice do not exhibit elevated peripheral blood reticulocytes, as measured by thiazole orange staining (Fig. 2B), consistent with a primary production defect rather than accelerated destruction associated with loss of E2F-2. We tested this supposition further by performing carboxyfluorescein succinimidyl ester (CFSE) labeling assays to measure the life span of circulating E2F-2 knockout RBCs. We found that E2F-2 knockout cells do not have a significantly altered life span compared to that of wild-type controls (Fig. 2C). Our findings suggest that the reduction in peripheral RBCs of E2F-2-null mice is not caused by accelerated destruction.

E2F-2 is required for efficient stress erythropoiesis. Comparison of absolute bone marrow erythroid cell (Ter119-positive) numbers in wild-type versus E2F-2-null animals at steady state revealed a significant reduction in the latter group (Fig. 3A). Notably, early erythroid progenitors (CFU-E and erythroid burst-forming units [BFU-E]) appear to be relatively insensitive to Rb/E2F pathway perturbations, with only modest changes in erythroid colony-forming cells apparent in both Rb knockout and cyclin E knock-in mice (5, 12). Moreover, loss of EKLF, which leads to near complete ablation of E2F-2 expression in the erythroid lineage, is not associated with significant depletion of CFU-E or BFU-E (16). Therefore, E2F-2 may regulate homeostasis of bone marrow erythroid cell numbers within the pool of more mature progenitors. We did not see evidence of significantly increased cell death in bone marrow erythroblasts in E2F-2 knockout mice (Fig. 3A, inset); thus, we considered the possibility that altered cell proliferation accounts for the absolute decrease in bone marrow erythroid cell numbers in these animals.

To more precisely understand the relationship of cell cycle dynamics to erythroid cell production in wild-type versus E2F-2 knockout mice, we studied stress erythropoiesis. The spleen is the major source of RBCs during stress erythropoiesis (27, 28). To compare stress erythropoiesis in wild-type and knockout mice, we exposed them to phenylhydrazine (PHZ) to induce hemolysis. We harvested peripheral blood and spleens at 7 and 11 days postinjection to study erythropoiesis during recovery from hemolytic injury. During stress erythropoiesis, loss of E2F-2 does not result in any obvious immunophenotypic differences in splenic terminal erythroid differentiation relative to wild-type controls (Fig. 3B). Seven days following PHZ injection, both wild-type and E2F-2 knockout mice demonstrate larger, more cellular spleens than untreated animals; however, E2F-2-null spleens exhibit fewer total and erythroid cells (Fig. 3C and D). After 11 days, E2F-2 knockout spleens still have lower total and $Ter119^+$ cell counts than wild-type spleens.

After stress, as in steady state (Fig. 2A), E2F-2-null mice have lower peripheral RBC counts than wild-type animals (Fig. 3E). In contrast to the case for steady-state erythropoiesis (Fig. 2B), E2F-2 knockout animals have significantly fewer reticulocytes in the peripheral blood during stress erythropoiesis (Fig. 3F).

We next examined cell cycle distributions in wild-type and E2F-2-null, $Ter119^+$ spleen cells. We found that E2F-2 knockout mice demonstrate increased numbers of cells in S phase and decreased cells in G_2/M phase following administration of PHZ (Fig. 3G to H). Moreover, with bromodeoxyuridine (BrdU) pulse-labeling of both PHZ-treated and untreated mice and subsequent calculation of S-phase duration (15, 29), we found significantly slower S-phase transit of E2F-2-null splenocytes both during stress erythropoiesis and at steady state. E2F transcription factors play well-defined roles in S-phase entry and progression (24, 25). Our findings suggest that reduced S-phase transit rates in erythroblasts due to E2F-2 loss impair homeostasis of erythroid cell populations.

E2F-2 regulates erythroid cell enucleation. Bone marrow immunophenotyping alone cannot resolve the final stages of erythroid cell maturation, as the gating

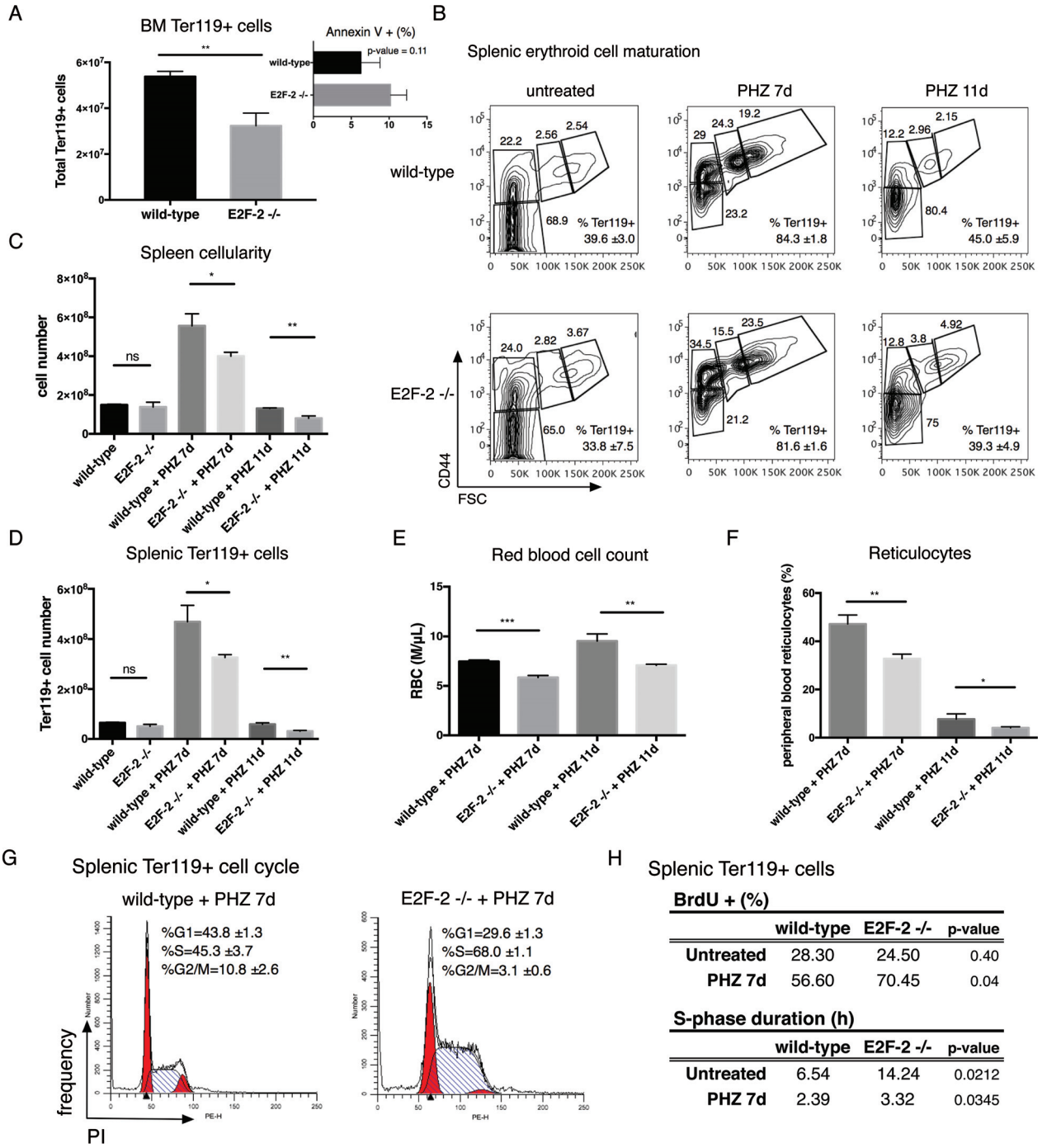

BrdU + (%)

	wild-type	E2F-2 -/-	p-value
Untreated	28.30	24.50	0.40
PHZ 7d	56.60	70.45	0.04

S-phase duration (h)

	wild-type	E2F-2 -/-	p-value
Untreated	6.54	14.24	0.0212
PHZ 7d	2.39	3.32	0.0345

FIG 3 E2F-2 regulates cell cycle progression during stress erythropoiesis. (A) Bone marrow cells from wild-type and E2F-2-null mice were harvested, manually counted, stained for Ter119$^+$ expression, and enumerated by flow cytometry. **, $P \leq 0.01$. Inset, Ter119$^+$ bone marrow cells were stained with anti-annexin V and 7-AAD and analyzed by flow cytometry, and the average percentages of annexin V-positive, 7-AAD-negative cells are displayed with corresponding standard deviations ($n = 3$ per genotype). (B) Age- and sex-matched wild-type and E2F-2 knockout animals were administered PHZ and their spleens harvested at 7 or 11 days postinjection. Representative splenic erythroid cell maturation profiles are shown, with the relative contributions of each cell subpopulation indicated. Total Ter119$^+$ splenocyte representations are listed with corresponding standard deviations ($n = 3$ per genotype and time point). (C) Splenocytes from mice of the indicated genotypes and treatment time points were manually counted. **, $P \leq 0.01$; *, $P \leq 0.05$; not significant (ns), $P > 0.05$. (D) Wild-type and E2F-2-null spleens were harvested as for panel B and stained for Ter119 expression, and positive cells were enumerated by flow cytometry. **, $P \leq 0.01$; *, $P \leq 0.05$; ns, $P > 0.05$. (E) Peripheral blood from animals treated as for panel A was collected and complete blood counts performed; RBC values are shown. ***, $P \leq 0.001$; **, P ≤ 0.01. (F) Reticulocytes were enumerated from peripheral blood collected as for panel D using thiazole orange staining. **, $P \leq 0.01$; *, $P \leq 0.05$ (using one-tailed *t* test). (G) Spleens from animals treated as for panel B were harvested, and cells were stained for Ter119 expression then labeled with propidium iodide for DNA content measurement to model cell cycle profiles. Shown are frequencies of cells in each cell cycle phase as an average from 3 animals. (H) Untreated animals or those treated with PHZ as for panel B were administered BrdU and spleens harvested 2 h later. Cells were stained for Ter119 expression and 7-AAD and BrdU incorporation and analyzed by flow cytometry. S-phase transit time was calculated as described previously (15, 29). Frequencies of BrdU$^+$ cells and S-phase durations are indicated as an average from 3 mice per genotype, with corresponding *P* values indicated.

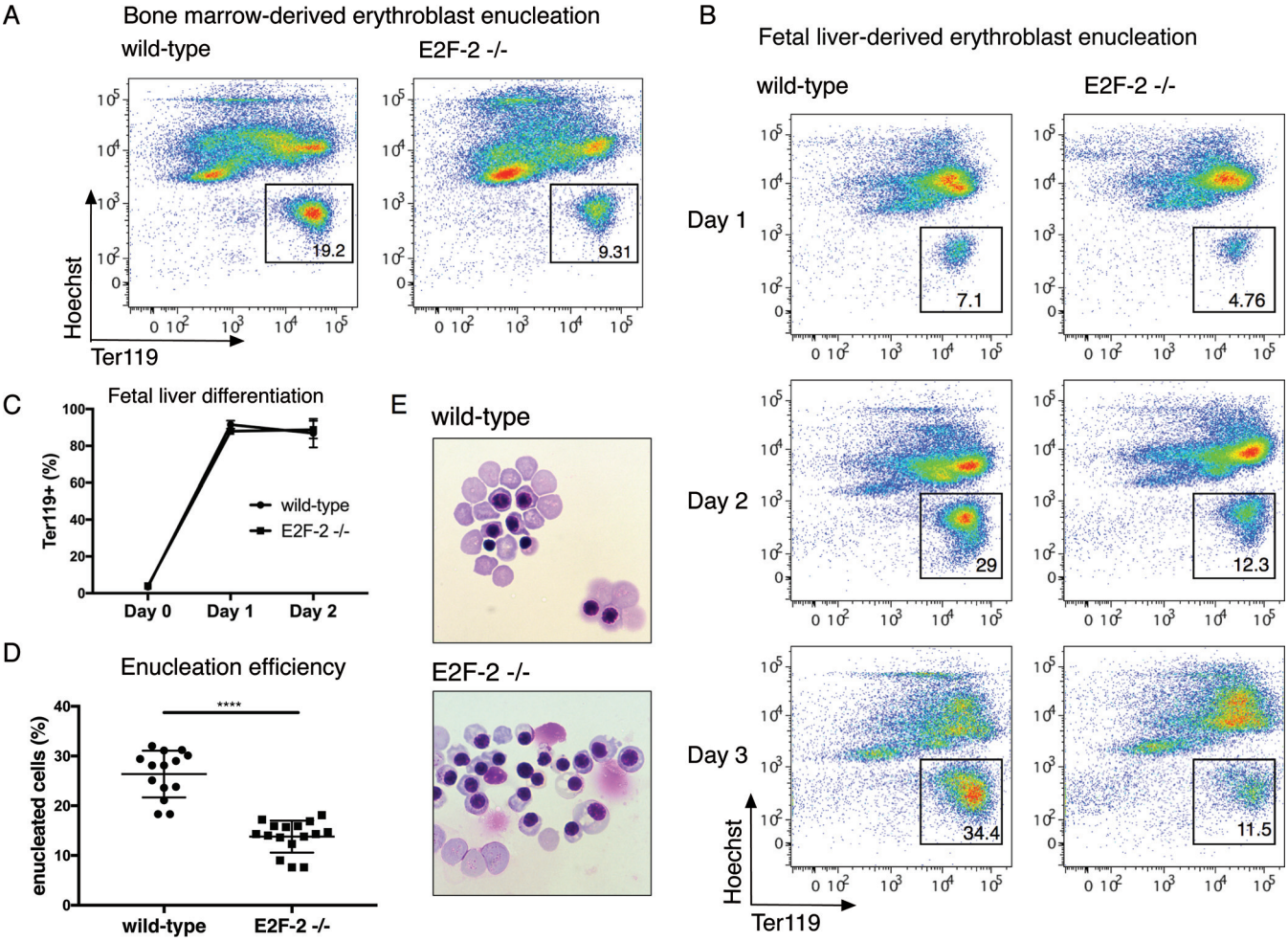

FIG 4 E2F-2 regulates erythroblast enucleation. (A) Hematopoietic progenitors were harvested from wild-type and E2F-2 knockout bone marrow, differentiated to the erythroid lineage in culture for 2 days, and stained with Hoechst 33342 and anti-Ter119 antibody. The plots shown are representative from an age- and sex-matched pair, with gates outlining the enucleated cell population (Ter119$^+$ and Hoechst negative). (B) Hematopoietic progenitors were obtained from E14.5 wild-type and E2F-2 knockout fetal livers and differentiated in culture from 1 to 3 days, and enucleation was analyzed as for panel A. (C) Hematopoietic progenitors (day 0) were directly stained for Ter119 expression following lineage depletion or following differentiation over the indicated time points. Shown is the average frequency of Ter119$^+$ cells at each time point with corresponding standard deviations ($n = 4$ mice). (D) Percentage of enucleated cells in fetal liver-derived erythroid cultures differentiated for 2 days, as described for panel B. Each symbol represents an individual experiment. ****, $P \leq 0.0001$. (E) Micrographs (magnification, ×40) of wild-type and E2F-2-null fetal liver erythroid cells, sorted based on CD44 versus FSC within the Ter119$^+$ population to obtain RIV cells.

strategies used to demarcate late-stage erythroblasts (population V) include a mix of nucleated and enucleated forms (Fig. 4E). Thus, in the absence of abnormal erythroblast maturation evidenced by immunophenotype or accelerated RBC destruction in *E2f2*-null mice, we hypothesized that the reduced level of RBCs in these animals during steady-state hematopoiesis is due to defective maturation beyond the orthochromatic erythroblast stage. To test this, we isolated lineage-depleted bone marrow cells and differentiated them to mature erythrocytes in culture to study enucleation. After 2 days, E2F-2 knockout cells show severely impaired enucleation compared to that of wild-type controls (Fig. 4A). Next, we used fetal liver-derived erythroid differentiation cultures (23) and evaluated erythroid cell enucleation over a three-day time course. Similar to what we observed in the bone marrow-derived cultures, after 2 days, E2F-2-null fetal liver-derived cells displayed defective enucleation (Fig. 4B, D, and E), while cells of both genotypes differentiated from Ter119 negative to Ter119 positive with similar kinetics (Fig. 4C). After an additional 24 h in culture, E2F-2 knockout cell cultures accumulated no further enucleated cells, consistent with the notion that enucleation in these cells is not simply delayed (Fig. 4B). Together, our results indicate that E2F-2 is required for normal erythroid cell enucleation.

A Differentially expressed genes

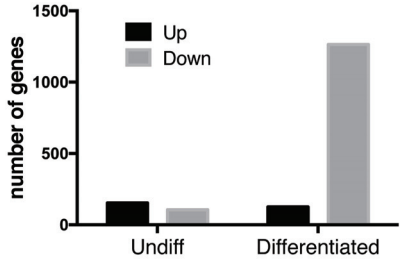

B Functional annotation (differentiated)

GO Term	Number of genes	FDR score
cell cycle	111	4.00E-22
response to DNA damage stimulus	61	7.40E-15
chromosome organization	64	1.10E-09
cellular response to stress	64	1.10E-09
organelle fission	41	2.50E-09
macromolecule catabolic process	84	2.30E-08
RNA processing	59	2.40E-06

C

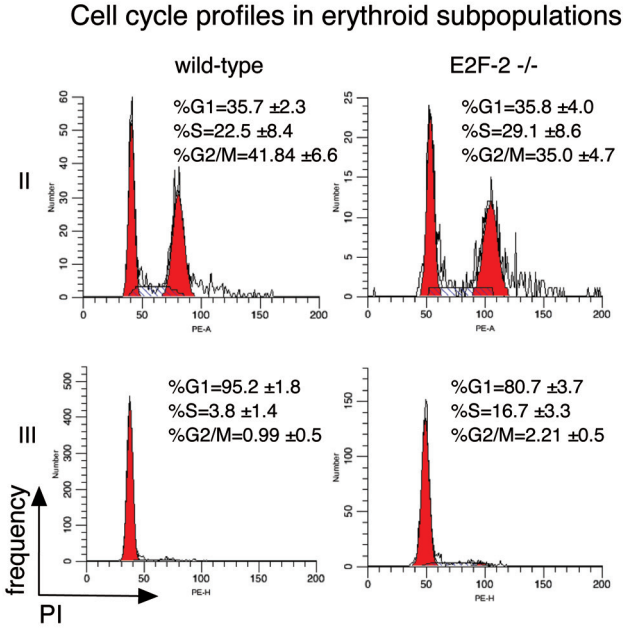

D

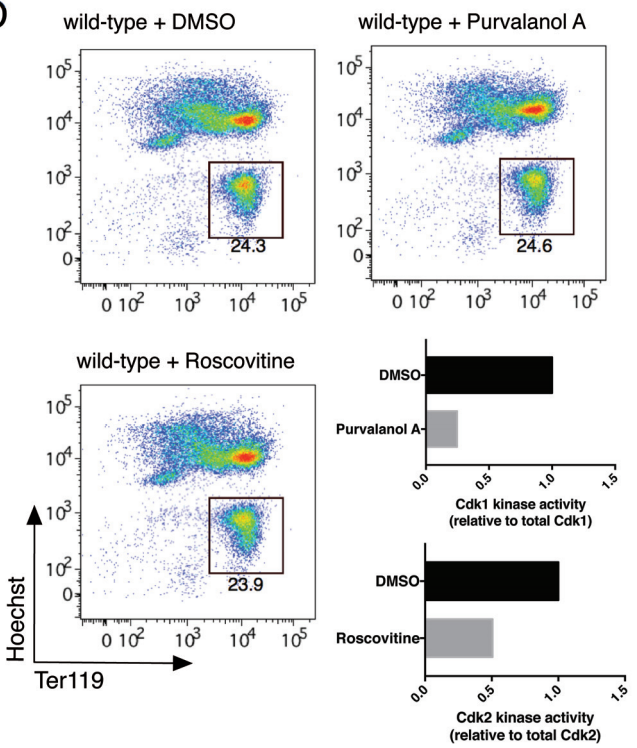

FIG 5 E2F-2 regulates cell cycle- and chromosome organization-related genes but does not alter cell cycle kinetics in terminally maturing erythroid subpopulations. (A) Hematopoietic progenitors were isolated from wild-type and E2F-2 knockout fetal livers (E14.5) and either harvested for RNA or differentiated in culture. Orthochromatic erythroblasts were collected and RNA harvested for RNA sequencing. Differentially expressed genes between E2F-2 knockout and wild-type samples were defined as those with a $\log_2$ fold change of $\geq$1. (B) Functional annotation analysis of differentially expressed genes in E2F-2 knockout erythroblasts was performed (NIH DAVID tool [30]), and shown are nonsynonymous, Gene Ontology (GO) biological process terms with a Benjamini-Hochberg (FDR) score of $<$1.0E$-$6. (C) Wild-type and E2F-2 knockout bone marrow cells were harvested, stained for Ter119 and CD44 expression, fixed, and labeled with propidium iodide for DNA content measurement for cell cycle profiles. Representative cell cycle profiles are shown for RII and RIII subpopulations. Cell cycle distributions are listed with standard deviations from three age- and sex-matched mice per genotype. (D) Left, wild-type fetal liver-derived progenitors were differentiated in culture to erythroid cells and treated with Cdk inhibitors (purvalanol A or roscovitine) during the final 14 h of the differentiation time course. Cells were collected and assayed for enucleation as for Fig. 4. Representative plots are shown. Right, fetal liver-derived progenitors were differentiated in culture for 1 day, and Cdk inhibitors were added and left for 14 h overnight. Cells were lysed, and histone kinase assays were performed.

Transcriptome profiling of E2F-2 knockout cells identifies widespread defects in gene expression during terminal differentiation. To help define the mechanism by which E2F-2 regulates erythroid cell enucleation, we first performed RNA sequencing on both lineage-depleted fetal liver progenitors and late-stage (orthochromatic) erythroblasts from wild-type and E2F-2 knockout cells. We verified that morphologically comparable cells from both genotypes were used in this assay by direct visualization. In undifferentiated progenitor cells, a limited number of genes change in expression between the wild-type and knockout cells. In differentiated erythroblasts, expression of relatively few genes is upregulated in knockout compared to wild-type cells, whereas over 1,200 genes are downregulated, consistent with a role for E2F-2 acting as a transcriptional activator during this stage of erythroid maturation (Fig. 5A). Taking the

findings together, we surmise that loss of E2F-2 does not result in widespread gene expression changes in undifferentiated cells, perhaps because other E2F family members are expressed at sufficient levels to compensate; however, in late-stage erythroblasts, loss of the dominant activator E2F results in profound misregulation of gene expression.

We performed functional annotation analysis using the NIH DAVID tool (30) on differentially expressed genes in E2F-2 knockout erythroblasts to identify major E2F-2-regulated pathways in these cells. As expected, many genes involved in cell cycle control, including well-known E2F targets such as *Ccne1*, were identified (Fig. 5B). Accordingly, we examined the cell cycle in discrete bone marrow erythroid cell subpopulations. In basophilic erythroblasts (RII), E2F-2 knockout cells show cell cycle distributions similar to those of wild-type controls, and with further maturation to polychromatic erythroblasts (RIII), both wild-type and knockout cells show comparable G_1 arrest profiles (Fig. 5C).

To assess whether E2F-2-regulated cyclin-Cdk complex activities might play a direct role in promoting erythroid cell enucleation, we treated fetal liver-derived erythroid cells with cyclin-dependent kinase (Cdk) inhibitors during the final 14 h of culture, when the largest amount of enucleation occurs (31). We utilized purvalanol A to inhibit Cdk1 (Cdc2) and roscovitine to inhibit Cdk2; these kinases complex with cyclins expressed significantly less (at the transcript level) in E2F-2 knockout erythroid cells, including cyclins E1, A2, and B1 (see Table S1 in the supplemental material). The addition of these Cdk inhibitors to fetal liver-derived cultures does not alter enucleation (Fig. 5D). Together, our data suggest that E2F-2-dependent control of cell cycle progression or downstream cyclin/Cdk activities is not critical for maturation of late-stage (basophilic erythroblasts and beyond) bone marrow erythroid cells during steady-state hematopoiesis.

E2F-2 loss results in impaired nuclear condensation during erythroblast enucleation. Erythroid cell enucleation is comprised of a number of distinct processes, including nuclear condensation, contractile actin ring (CAR) formation, and nuclear polarization. Having identified differential expression of genes involved in chromosome organization, including a number of genes involved in chromatin condensation (Fig. 5B; see Table S1 in the supplemental material), we first wanted to understand the consequences of E2F-2 loss for nuclear condensation during terminal erythroid maturation. We measured the nuclear area of DAPI (4′,6′-diamidino-2-phenylindole)-stained, differentiated E2F-2-null and wild-type cells using confocal microscopy. Loss of E2F-2 results in significantly larger nuclei than in wild-type controls (Fig. 6A), indicating that E2F-2 regulates erythroblast nuclear condensation. To examine this phenomenon over a greater number of cells, we used imaging flow cytometry to measure the nuclear area of DRAQ5-labeled cells. Excluding nonerythroid, enucleating, or enucleated cells, samples were gated on Ter119 and DRAQ5 double-positive cells with a spherical aspect ratio to ensure comparison of morphologically similar cells. In agreement with the confocal data, E2F-2 knockout erythroid cells have larger nuclei, both in aggregate and with comparison of individual erythroblast subpopulations (Fig. 6B).

Another process critical for erythroblast enucleation is CAR formation, which requires actin and myosin to interface at the location in which the nucleus will be expelled from the cell. Using confocal microscopy, we directly visualized and enumerated CARs in fetal liver erythroblast cultures and found that E2F-2-depleted erythroblasts form these structures at a frequency similar to that for wild-type cells (Fig. 6C).

As an additional step toward nuclear extrusion and reticulocyte formation, the erythroid cell nucleus polarizes to the eventual site of exclusion. Nuclear polarity can be quantified using imaging flow cytometry by calculating the delta centroid value, which measures the separation between the centers of corresponding bright-field and DRAQ5 images, such that a larger delta centroid value indicates a more polarized nucleus. As a control for variation in nuclear area, we divided the delta centroid value by the radius of the DRAQ5 image. With this analysis, we observed an obvious polarization as cells

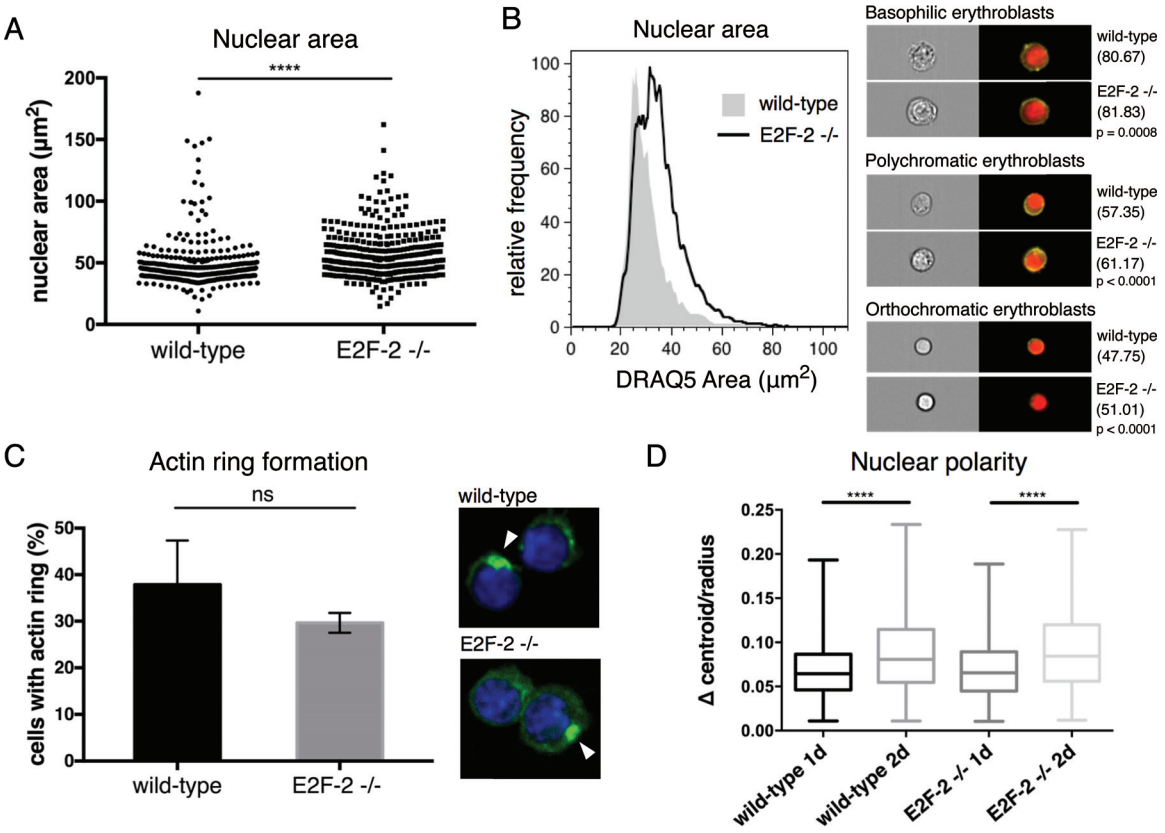

FIG 6 E2F-2 regulates nuclear condensation during erythroid enucleation. (A) Fetal liver-derived progenitor cells from wild-type and E2F-2-null mice were differentiated for 2 days in culture. Cells were placed on polylysine-coated coverslips by cytospins and stained with DAPI. Confocal z-stack images were acquired, and the nuclear area was calculated from maximally projected images; each symbol represents an individual nucleus. Approximately 400 nuclei per genotype were analyzed from at least two biological replicates ($P < 0.0001$ using the Mann-Whitney test). (B) Wild-type and E2F-2-null fetal liver-derived erythroid cells were fixed, stained with anti-Ter119 antibody and DRAQ5, and analyzed using imaging flow cytometry. Left, representative histograms of DRAQ5 area measurements for each genotype; at least 10,000 events were collected per experimental condition. Right, representative bright-field and DRAQ5 (red)/Ter119 (yellow) images of wild-type and E2F-2-null erythroid cells within indicated erythroid subpopulations, gated using Ter119 and cell size as described previously (37). Mean nuclear area measurements for each genotype are displayed on the right with corresponding P values. (C) Wild-type and E2F-2 knockout fetal liver-derived erythroid cells were cultured, differentiated, fixed, and stained with Alexa Fluor-488-conjugated phalloidin and DAPI. Cells were imaged, and actin ring formation was counted. Left, frequencies of cells with an actin ring are shown for both genotypes; over 500 cells were counted per genotype from 4 separate experiments ($P = 0.142$). Right, representative images of actin rings (arrowheads) in wild-type and E2F-2 knockout cells. (D) Wild-type and E2F-2-null fetal liver-derived erythroid cells were differentiated for 1 or 2 days, fixed, and stained as for panel B. A minimum of 10,000 events per experimental condition were collected using imaging flow cytometry. Delta centroid values were calculated and corrected for variations in nuclear size by dividing by the DRAQ5 radius. ****, $P \leq 0.0001$.

differentiated between 1 and 2 days in both wild-type and E2F-2-null erythroid cultures, with the E2F-2 knockout exhibiting no defects in polarization (Fig. 6D). Taken together, these data suggest that E2F-2 regulates nuclear condensation during erythropoiesis, with defective condensation in E2F-2 knockout cells resulting in impaired enucleation.

***Cit*, encoding citron Rho-interacting kinase, is a direct E2F-2 target that is induced during erythroid differentiation.** To determine the mechanism by which E2F-2 regulates nuclear condensation and subsequent erythroid enucleation, we focused on genes deregulated in E2F-2 knockout differentiated erythroid cells that were associated with chromosome organization (see Table S1 in the supplemental material). We found that citron Rho-interacting kinase (CRIK), which plays an established role in late mitosis and cytokinesis (32–36), is induced over the course of differentiation from wild-type progenitors to orthochromatic erythroblasts. Notably, *Cit* gene expression decreases in E2F-2 knockout erythroid cells (Fig. 7A). Moreover, using the fetal liver culture system, we compared CRIK protein levels between progenitor and Ter119$^+$ cells. In agreement with our RNA sequencing data, CRIK protein is induced during

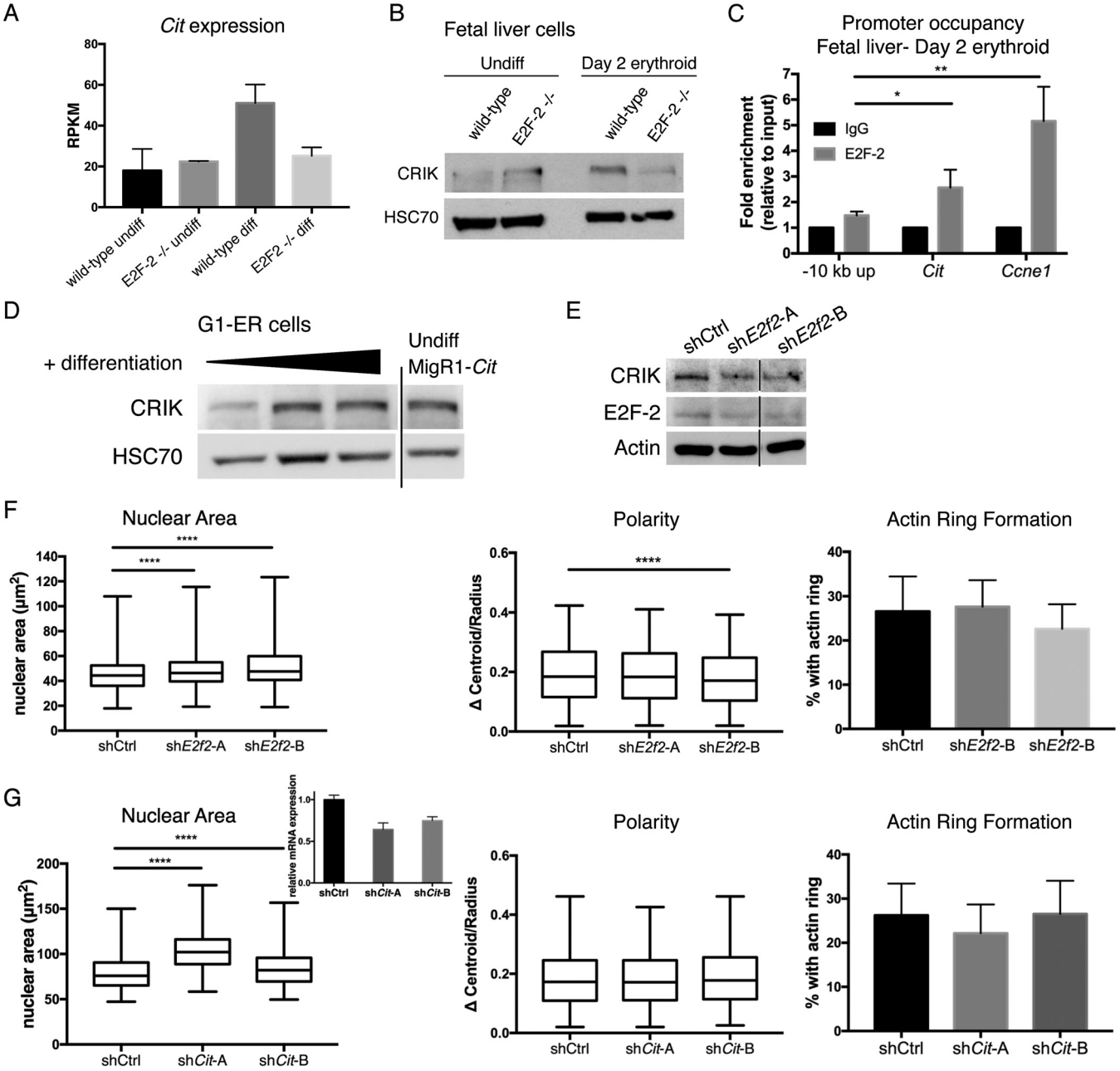

FIG 7 *Cit* expression is directly regulated by E2F-2 during erythroblast differentiation and controls nuclear condensation. (A) Calculated reads per kilobase per transcript per million mapped reads (RPKM) from RNA sequencing (described for Fig. 5A) for *Cit* are shown; values represent averages from two biological replicates, and error bars represent standard deviations. (B) Fetal liver-derived hematopoietic progenitors and differentiated, purified Ter119$^+$ cells of the indicated genotypes were harvested and immunoblotted for CRIK. A representative Western blot is shown; HSC70 was used as a loading control. (C) E2F-2 chromatin immunoprecipitation was performed on wild-type fetal liver-derived erythroid cells. Real-time quantitative PCR was performed with primers 10 kb upstream of *Cit* (negative control) and at *Cit* and *Ccne1* promoters. *Ccne1* is shown as a canonical E2F target for comparison (26). Values shown are averages from 4 experiments with corresponding standard deviations. **, $P \leq 0.01$; *, $P \leq 0.05$. (D) β-Estradiol was added to G1-ER cells to induce differentiation over 24 h. Cells were removed during the course of differentiation, lysed, and immunoblotted for CRIK; HSC70 is shown as a loading control. Undifferentiated G1-ER cells were retrovirally transduced with MigR1-*Cit* and immunoblotted in parallel for expression comparison. The splice mark indicates irrelevant samples from the same gel. (E) G1-ER cells were retrovirally transduced with a control shRNA (shCtrl) or one of two hairpins designed to target *E2f2*. Cells were immunoblotted for E2F-2 and CRIK expression, with β-actin shown as a loading control. Samples were run on a single gel. (F) G1-ER cells were transduced as described for panel E, fixed, stained with anti-Ter119 antibody and DRAQ5, and analyzed using imaging flow cytometry ($\geq$10,000 events per sample). Cells were gated based on GFP and DRAQ5 staining and spherical aspect ratio. Left, nuclear area was measured as the area of the Draq5 image as for Fig. 6 (****, $P \leq 0.0001$). Middle, nuclear polarity was measured by imaging flow cytometry as for Fig. 6. One hairpin, sh*E2f2*-B, showed a significant reduction in polarity ($P < 0.0001$). Right, transduced G1-ER cells were imaged for actin ring formation as for Fig. 6. Actin rings were enumerated in at least 150 cells per sample; no significant differences were found between shCtrl and sh*E2f2* samples. (G) G1-ER cells were retrovirally transduced with shCtrl or one of two hairpins targeting *Cit*. Cells were harvested for RNA, and quantitative reverse transcription-PCR was performed. Left, inset, *Cit* mRNA expression values relative to *Rn18s*. Left, nuclear area ($P < 0.0001$). Middle, nuclear polarity; no-sh*Cit* samples showed a significant reduction in polarization. Right, actin rings were enumerated; no significant differences were observed.

wild-type erythroid differentiation, while differentiated E2F-2-null cells exhibit reduced CRIK expression (Fig. 7B). To determine if *Cit* is a direct transcriptional target of E2F-2, we performed E2F-2 chromatin immunoprecipitation and quantitative PCR (ChIP -qPCR) in primary differentiated fetal liver-derived erythroid cells. Increased enrichment of E2F-2 at the *Cit* promoter, compared to IgG, indicates that E2F-2 directly regulates *Cit* gene expression in differentiated erythroid cells (Fig. 7C). CRIK interacts with Rac GTPases, which are known to regulate erythroid cell enucleation (31, 37). A different Rho/Rac-regulated kinase, mDia2, is also described as being required for efficient enucleation (31). Thus, we hypothesized that E2F-2-dependent induction of *Cit* expression promotes erythroid enucleation.

Cit expression and CRIK activity regulate erythroblast nuclear condensation and enucleation. In G1E-ER4 (G1-ER) cells, an embryonic stem cell-derived *Gata1*-null hematopoietic progenitor line that expresses the GATA-1–ER fusion protein, we were able to attain stable partial knockdown of *Cit* using short hairpin RNA (shRNA) (Fig. 7G). Although differentiating G1-ER cells demonstrate significant overlap in gene expression with primary erythroblasts (38–40), these cells do not undergo efficient enucleation. However, G1-ER cells undergo nuclear condensation and polarization and form CARs during differentiation. We first determined that CRIK expression is induced during G1-ER cell differentiation (Fig. 7D) and that CRIK expression is partially sensitive to E2F-2 levels, using shRNA targeting *E2f2* (Fig. 7E). We then quantified the nuclear area in G1-ER cells expressing *Cit* or *E2f2* shRNA and found that upon knockdown of either, the nuclear area increased compared to that of control hairpin-expressing cells (Fig. 7F and G). In contrast, neither *Cit* nor *E2f2* knockdown consistently affected nuclear polarization or CAR formation (Fig. 7F and G).

We next assayed phosphorylation of myosin regulatory light chain 2 (pMLC2), a known CRIK kinase substrate (41), in primary E2F-2-null erythroblasts and found that this is significantly reduced compared to that in wild-type cells, providing evidence of reduced CRIK enzymatic activity in the absence of E2F-2 (Fig. 8A). We then used pharmacologic inhibitors to assess the consequences of inhibiting CRIK activity for erythroid cell enucleation in wild-type fetal liver-derived erythroblasts. Because there are no known CRIK-specific inhibitors, we used two kinase inhibitors, A-674563 and RAF265, which inhibit AKT and RAF, respectively, and share CRIK alone as a common target, both at micromolar concentrations (42). We treated fetal liver cultures with each inhibitor during the final 14 h of maturation to study their effect at a time when erythroid cells had stopped proliferating. Treatment of wild-type fetal liver cells with both A-674563 and RAF265 resulted in impaired enucleation (Fig. 8B). We confirmed that A-674563 and RAF265 both inhibited MLC2 phosphorylation (Fig. 8C). To further demonstrate specificity of the prior kinase inhibitor experiments for CRIK inhibition, we also treated cells with MK-2206, an AKT-specific inhibitor (43, 44). Treatment with this inhibitor elicits an effect on neither nuclear area nor MLC2 phosphorylation (Fig. 8C and D).

Consistent with our hypothesis that CRIK is a downstream mediator of E2F-2-dependent control of erythroid cell enucleation, we also found that addition of either kinase inhibitor to wild-type erythroblasts resulted in a significant nuclear condensation defect, with accumulation of cells with larger nuclei as measured by imaging flow cytometry. In contrast, only A-674563 treatment partially impaired erythroblast nuclear polarization (Fig. 8D). Finally, to demonstrate functional significance of E2F-2-dependent CRIK regulation during erythroblast enucleation, we studied enucleation of wild-type and E2F-2-null erythroblasts following enforced expression of full-length *Cit* cDNA (Fig. 7D). In these assays, we observed partial but significant improvement of enucleation with *Cit* overexpression in knockout cells, while wild-type cells were unaffected (Fig. 8E). *In toto*, our experiments support the conclusion that CRIK activity is a critical downstream mediator of E2F-2-dependent control of erythroblast enucleation.

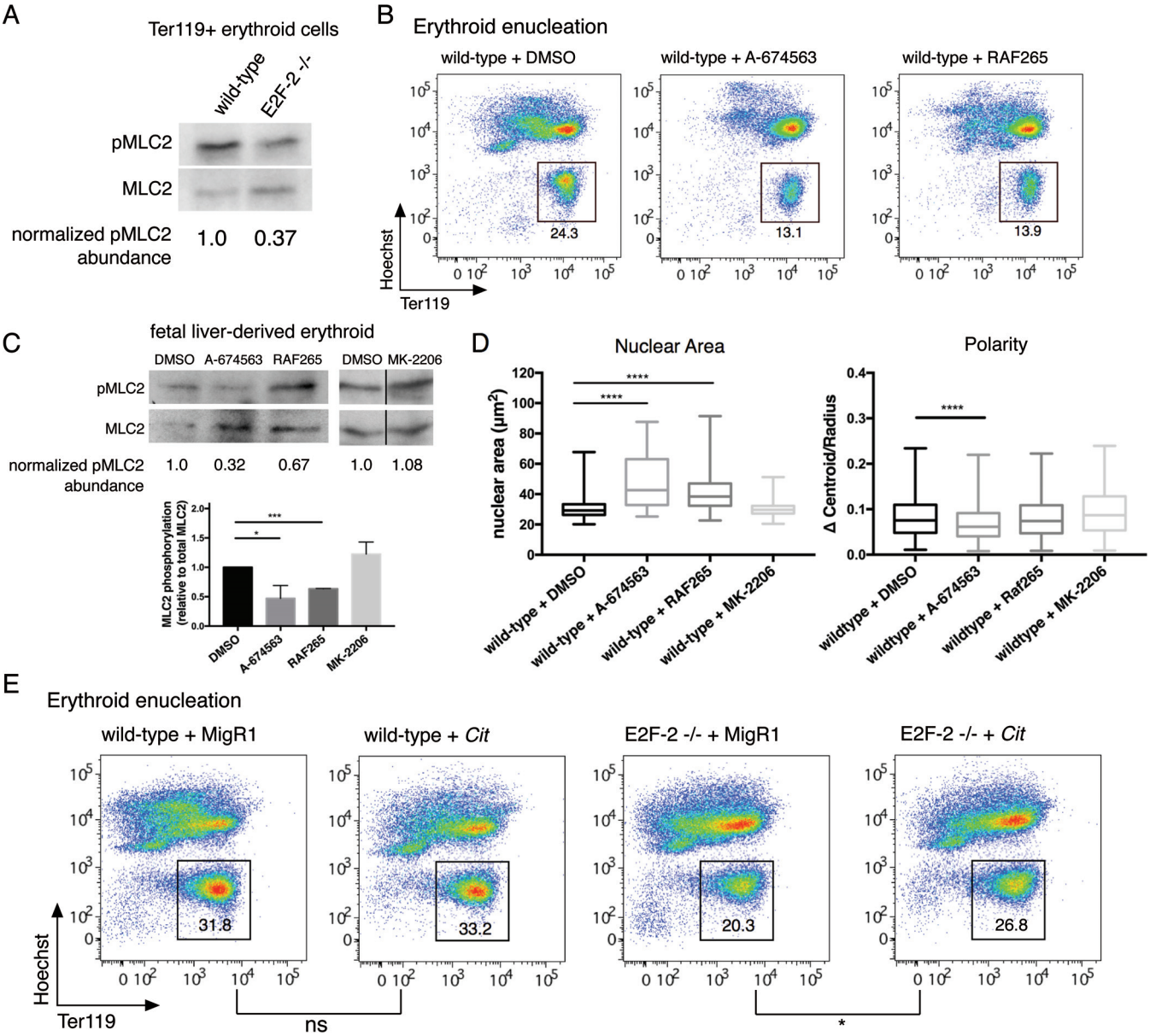

FIG 8 CRIK activity regulates erythroblast condensation and enucleation. (A) Wild-type and E2F-2$^{-/-}$ fetal liver-derived Ter119^{+} erythroid cells were immunoblotted for total myosin regulatory light chain 2 (MLC2) and phospho-T18/S19 MLC2 (pMLC2). Shown is a representative blot; pMLC2 abundance was quantified in ImageJ relative to total MLC2 levels, with normalized values indicated. (B) Wild-type fetal liver-derived cells were differentiated for 2 days in culture. Kinase inhibitors (A-674563 and RAF265; concentrations are listed in Materials and Methods) were added during the final 14 h of culture. Enucleation was assayed as for Fig. 4. (C) Wild-type fetal liver-derived erythroid cells were treated with kinase inhibitors and an AKT-specific inhibitor (MK-2206) for panel B. Cells were immunoblotted for total and phospho-MLC2 expression. Representative blots are shown, with the splice mark indicating removal of lanes containing cell lysates treated with lower concentrations of MK-2206. Bottom, immunoblots were quantified as for panel A; error bars represent standard deviations. ***, $P \leq 0.001$; *, $P \leq 0.05$; there was a nonsignificant difference in pMLC2 abundance with MK-2206. (D) Wild-type fetal liver-derived erythroid cells were treated as described for panel B. Cells were fixed, stained with anti-Ter119 antibody and DRAQ5, and analyzed using imaging flow cytometry. Nuclear area was measured by the area of the DRAQ5 stain. ****, $P \leq 0.0001$; ns, $P > 0.05$. Nuclear polarity was measured as for Fig. 6. ****, $P \leq 0.0001$; ns, $P > 0.05$. (E) Wild-type and E2F-2$^{-/-}$ fetal liver-derived hematopoietic progenitors were transduced with empty vector (MigR1) or MigR1-*Cit*. Cells expressing MigR1-*Cit* exhibited approximately 2-fold overexpression of *Cit*, measured by quantitative reverse transcription-PCR. Transduced cells were differentiated for 2 days, and enucleation was measured within the GFP^{+} population. E2F-2$^{-/-}$ cells showed a significant increase in enucleation compared to MigR1 controls (*, $P = 0.03$ [three separate experiments]); a significant difference was not observed for *Cit*-expressing wild-type cells compared to MigR1.

DISCUSSION

E2F-2 is a ubiquitously expressed transcription factor with canonical functions in the promotion of cell cycle progression following its release from Rb-imposed negative regulation (24, 25). Consistent with a role for E2F-2 as a critical mediator of Rb pathway control during terminal erythroid maturation, we found that E2F-2 deletion rescues

deregulated cyclin E-Cdk2-associated erythroid maturation defects *in vivo* as evidenced by relative frequencies of bone marrow basophilic to orthochromatic erythroblasts (Fig. 1D). However, E2F-2 knockout, cyclin $E^{T74A\ T393A}$ mice remain anemic, underscoring the requirement for basal E2F-2 activity during late-stage erythropoiesis. Based on our analysis of stress erythropoiesis in wild-type and E2F-2 knockout mice, we find that E2F-2 regulates cell cycle progression in splenic erythroid cells and thus is required for efficient red cell production (Fig. 3). Our detailed study of steady-state erythropoiesis demonstrates that loss of E2F-2 impairs enucleation (Fig. 4A). Although a prior study of fetal erythropoiesis that examined embryonic day 13.5 (E13.5) peripheral erythroid cells did not describe an enucleation phenotype in E2F-2 knockout embryos (8), we note that the circulating erythroid cells were not distinguished on the basis of their ultimate cell of origin. Indeed, circulating RBCs at this developmental stage are a mixture of primitive yolk sac-derived and definitive aorta-gonad-mesonephros (AGM)-derived cells (45). In contrast, the assays of erythroid cell enucleation we employ, similar to those used by many other groups (31, 46–48), utilize bone marrow- and fetal liver-derived hematopoietic progenitors, both of which are definitive AGM-derived cells. Importantly, in both sets of assays (Fig. 4A and B), we found that E2F-2 loss significantly impairs enucleation.

By dissecting enucleation into discrete components, we identified a previously unrecognized function for E2F-2 in the promotion of nuclear condensation (Fig. 6). Using RNA sequencing to compare the transcriptomes of E2F-2 knockout and wild-type progenitors and differentiated erythroblasts, we found E2F-2-dependent erythroid induction of CRIK, a mitotic kinase known to interact with Rho family GTPases, which are linked to the control of enucleation (31, 37). In mitotic cells, CRIK regulates astral microtubule length and spindle orientation (36), and during cytokinesis, CRIK colocalizes with RhoA and mediates contractile function at the cleavage furrow (32, 33, 35). Previous studies of erythroid enucleation describe a critical role for Rac GTPases in organizing CAR formation and lipid raft clusters between the pyrenocyte and incipient reticulocyte (37). One known target of CRIK activity is MLC2, and interestingly, myosin colocalizes to the CAR during erythroid enucleation (37). However, we did not observe a difference in CAR formation in E2F-2 knockout erythroid cells (Fig. 6C) or with *Cit* or *E2f2* knockdown (Fig. 7F and G). As CRIK is partially inhibited in all of these experimental contexts, these data are consistent with the concept that CAR function during erythroid enucleation may be more sensitive to modulation of CRIK activity levels than CAR formation *per se*. Alternatively, we speculate that during erythroid cell enucleation, CRIK may utilize a distinct set of interacting proteins (49) to properly maintain nuclear condensation, enabling efficient enucleation. In future studies, *in vivo* imaging of endogenous CRIK localization and identification of its binding partners in enucleating erythroid cells will aid our understanding of mechanisms by which CRIK regulates nuclear condensation.

Our findings implicate E2F-2 in regulating the expression of mitotic kinases that are adapted to perform specialized functions in nuclear condensation and enucleation. This particular role for E2F-2 may explain why it is expressed at high levels during late-stage erythroid maturation (Fig. 1). Moreover, our results provide context for interpreting recent studies demonstrating that EKLF-dependent expression of cyclin/Cdk-inhibitory proteins (CDKIs) is required for efficient erythroblast enucleation (4), as CDKIs are likely to be critical inhibitors of cell cycle reentry in terminally differentiated cells that retain E2F transcriptional activity. A systems-based view of the molecular processes underlying enucleation will enable further understanding of the extent to which mitotic regulatory mechanisms are repurposed to promote this key component of terminal erythroid maturation.

MATERIALS AND METHODS

Mice. Generation of the *Ccne1*$^{T74A\ T393A}$ (cyclin $E^{T74A\ T393A}$ or cyclin E knock-in) and *E2f2* knockout mice was previously described (9, 12). E2F-2 knockout, cyclin $E^{T74A\ T393A}$ mice were generated by crossing homozygous mice in C57BL/6 backgrounds. Phenylhydrazine (PHZ) (Sigma-Aldrich) was administered by intraperitoneal (i.p.) injection at a dose of 90 mg/kg. Bromodeoxyuridine (BrdU) (BD Biosciences) was

administered i.p. (150 μl of a 10-mg/ml sterile stock solution). The Northwestern University and Medical College of Wisconsin IACUCs approved all mouse studies. All mice were genotyped by PCR as described in published protocols.

Cell culture. E14.5 fetal livers were harvested from wild-type and E2F-2 knockout dams and differentiated into erythroid cells as previously described with minor modifications (23). Briefly, fetal liver cells were lineage depleted using a customized EasySep mouse hematopoietic progenitor enrichment kit with a custom antibody cocktail (CD5, CD19, CD45R, Gr1, Ter119, 7-4, and CD8; StemCell Technologies). Next, cells were cultured overnight in Iscove modified Dulbecco medium (IMDM) (Life Technologies) supplemented with 15% fetal bovine serum (FBS), 10^{-4} M β-mercaptoethanol, 100 U/ml penicillin-streptomycin, 2 mM L-glutamine, CHO-KL conditioned medium (1:200), and 10 ng/ml murine recombinant interleukin-3 (IL-3) (Peprotech). Following expansion, cells were split into fibronectin (BD Biosciences)-coated plates and differentiated for 48 h in IMDM supplemented with 15% FBS, 1% bovine serum albumin (BSA), 10 μg/ml insulin, 200 μg/ml holotransferrin, 10^{-4} M β-mercaptoethanol, 100 U/ml penicillin-streptomycin, 2 mM glutamine, and 2 U/ml erythropoietin (Amgen). Pharmacologic inhibitors were added to culture media for the final 14 h of differentiation at the following concentrations: roscovitine (Sigma-Aldrich), 20 μM; purvalanol A (Sigma-Aldrich), 15 μM; A-674563 (Selleck Chemical), 20 μM; RAF265 (Selleck Chemical), 50 μM; and MK-2206 (Selleck Chemical), 10 μM. Bone marrow cells were harvested from adult mouse bilateral femurs and tibiae and cultured as described above.

G1E-ER4 (G1-ER) cells were cultured in IMDM supplemented with 15% FBS, 2% penicillin-streptomycin, 1:100,000 monothioglycerol (Sigma-Aldrich), 2 U/ml erythropoietin, and CHO-KL conditioned medium (1:200). To differentiate, 10^{-7} M β-estradiol was added to culture media for 48 h. Retroviral supernatants were prepared by transfecting Phoenix cells (G. Nolan, Stanford) using calcium phosphate precipitation. G1-ER cells were spinoculated with retroviral supernatants for 90 min at room temperature (RT).

Plasmids and antibodies. Antibodies used for flow cytometry were allophycocyanin (APC)- or APC Cy7-conjugated CD44 (IM7) and phycoerythrin (PE)-, fluorescein isothiocyanate (FITC)-, or APC-conjugated Ter119, all purchased from BD Biosciences. Antibodies used in immunoblots and chromatin immunoprecipitations were purchased as follows: anti-E2F-1 (KH95), E2F-2 (C-20), E2F-3 (C-18), E2F-4 (C-20), HSC70 (B-6), Cdk1 (Cdc2) (p34), and Cdk2 (M2), all purchased from Santa Cruz Biotechnology; Thr18/Ser19-phosphorylated myosin regulatory light chain 2 (pMLC2) and total MLC2 (D18E2), purchased from Cell Signaling Technology; beta-actin (AC-15; Sigma-Aldrich); CRIK (Proteintech); affinity-purified polyclonal anti-cyclin E (provided by Bruce Clurman, Fred Hutchinson Cancer Research Center, Seattle, WA); and anti-HDAC2 (3F3; Upstate). Whole-cell lysates were prepared in Nonidet P-40 buffer (0.5% Nonidet P-40 substitute, 10 mM Tris [pH 7.4], 0.15 M NaCl), with 10 mg/ml each of aprotinin, leupeptin, and pepstatin A, 50 mM sodium fluoride, and 1 mM sodium vanadate. Protein concentrations were quantified using the Bradford protein assay (Bio-Rad), and normalized lysates were electrophoresed and transferred to nitrocellulose membranes. Lysates were immunoprecipitated for Cdk1 and Cdk2, and kinase assays were performed as previously described (14). Short hairpin RNAs were designed to target *Cit* or *E2f2* using the GenScript siRNA design tool and subcloned into the Banshee-green fluorescent protein (GFP) vector for expression under the control of the H1 promoter. *Cit* full-length cDNA was cloned from caudal mouse embryo tissues (E14.5) using LongAmp *Taq* DNA polymerase (New England BioLabs) and stably expressed in hematopoietic progenitors using the MigR1 retroviral vector.

Hematopoietic cell analyses. Bone marrow and spleens were harvested from age- and sex-matched mice and resuspended in phosphate-buffered saline (PBS) with 2% FBS prior to immunophenotyping. For Western blot analysis of highly defined erythroid subpopulations, bone marrow cells were stained for surface marker expression and sorted using a FACS Aria cell sorter (BD Bioscience). Complete blood counts were obtained using peripheral blood collected from tail veins on a Scil Vet ABC hematology analyzer (Scil Animal Care Company). Peripheral blood was stained with thiazole orange (0.1 μg/ml) to enumerate reticulocytes.

Erythrocyte life span determination was performed as previously described (13). RBCs from wild-type or E2F-2-null mice were collected from peripheral blood obtained by cardiac puncture immediately after euthanization. RBCs were labeled with 10 μM carboxyfluorescein succinimidyl ester (CFSE) (Life Technologies) for 30 min at 37°C, washed, and resuspended in sterile PBS. Wild-type recipient mice received 1×10^9 labeled cells via retro-orbital injection. Peripheral blood was collected from tail veins at various time points and analyzed by flow cytometry.

Flow cytometry. For cell cycle studies, bone marrow or spleen cells were antibody stained, fixed in 2% formaldehyde in PBS for 10 min at RT, and stained with propidium iodide solution containing 10 μg/ml propidium iodide and 10 U/ml RNase A (Sigma-Aldrich). For BrdU labeling studies, spleens were harvested from PHZ-treated or untreated mice 2 h after BrdU injection, and incorporation was detected using the BrdU Flow kit (BD Biosciences). S-phase transit time was calculated based upon relative movement of BrdU-positive cells and mean fluorescence intensities of G_1 and G_2 populations, determined by 7-aminoactinomycin D (7-AAD) signal (15, 29). To measure enucleation, fetal liver or bone marrow cultures were stained with anti-Ter119 antibody and Hoechst 33342 (Life Technologies) for 15 min at RT in the dark. Annexin V staining utilized anti-annexin V antibody and associated detection reagents (BD Bioscience). All flow cytometry was performed on an LSRII flow cytometer (BD Bioscience) and analyzed using FlowJo (Tree Star). Cell cycle profiles were modeled using ModFit LT (Verity).

For imaging flow cytometry, 2×10^6 cells were stained with Ter119-PE (1:100; fetal liver cells only) for 30 min at 4°C. Next, cells were fixed with 4% formaldehyde in PBS for 20 min at RT and washed with PBS plus 2% FBS. Cells were resuspended in 100 μl of PBS with 2% FBS containing 5 μM DRAQ5 (eBioscience) and analyzed on an ImageStream X Mark II (Amnis). Analysis was performed using IDEAS (Amnis/Millipore). Samples were gated on Ter119 and DRAQ5 double positives. Cells were also gated on

bright-field gradient root mean squared (to select images that were in focus) and spherical erythroblasts as measured by an aspect ratio close to 1. Nuclear size was measured by area of the DRAQ5 image. Nuclear polarity was quantified by measuring the delta centroid between bright-field and DRAQ5 images and dividing by the radius of the corresponding DRAQ5 image.

Immunofluorescence. Differentiated fetal liver cells (10^5) were resuspended in PBS plus 2% FBS and cytospun to poly-L-lysine (Sigma)-coated coverslips at 350 rpm for 5 min (Shandon CytoSpin III). Adherent erythrocytes were fixed in 4% formaldehyde in PBS for 20 min and washed in PBS containing 0.1 M glycine (rinsing buffer). Cells were permeabilized in PBS containing 0.25% Triton X-100 (Sigma) for 5 min and rinsed twice before blocking in 1% BSA in PBS overnight at 4°C. Coverslips were stained in blocking solution for F-actin with Alexa Fluor 488-conjugated phalloidin (0.25 U/slide; Life Technologies) for 1 h. After being washed thrice with PBS, cells were incubated for 5 min at RT in PBS with 1 mg/ml DAPI (Sigma) and washed. Coverslips were mounted using Vectashield antifade (Vector Laboratories) or ProLong Gold antifade (Life Technologies) mounting medium. Imaging was performed with an Olympus Fv1000 MPE multiphoton laser scanning microscope with a 60× water immersion objective lens (1.20 numerical aperture) and Olympus FluoView acquisition software. For actin ring counting, phalloidin and DAPI images were acquired with 2× digital zoom at a rate of 20 μs/pixel. Images were later adjusted for brightness and contrast with Fiji image analysis software (50), and actin ring formation was quantified.

To quantify nuclear area for condensation analysis, z-stack DAPI images of greater than 20 slices (0.51 μm/slice) were acquired at a rate of 12.5 μs/pixel. Using Fiji, each stack was maximally projected and converted to an 8-bit image for further processing. We applied a threshold using the Huang dark algorithm (51). Following a conversion to binary, we performed watershed segmentation (52) to identify individual nuclei, which were measured for area using the Analyze Particles function. We queried each identified particle to the original DAPI-stained maximal projection to exclude any region of nonsingular nuclear identity from our analysis.

RNA sequencing. Fetal liver-derived progenitors (undifferentiated) were collected in TRIzol (Thermo Fisher Scientific) after lineage depletion as described above. Differentiated fetal liver cells were antibody stained, sorted on a FACS Aria cell sorter (BD Biosciences) to collect orthochromatic erythroblasts (Ter119- and CD41-positive, FSC-middle population), and collected in TRIzol. Total RNA was extracted from TRIzol and quantified using a Qubit fluorometer (Thermo Fisher Scientific). RNA was sent to BGI (Hong Kong) for library preparation, RNA sequencing on an Ion Torrent (Thermo Fischer Scientific) with at least 20 million reads per sample, and standard bioinformatics analysis. Differentially expressed genes were identified based on filtering those with a $\log_2$ fold change of >1.0 and a read per kilobase per transcript per million mapped reads (RPKM) cutoff value of 1 in at least one sample between E2F-2-null and wild-type samples.

ChIP. Following differentiation, 2×10^7 cells were fixed for 10 min at room temperature with 1% formaldehyde, and cross-linking was quenched with 125 mM glycine for 5 min. Cell pellets were resuspended in shearing buffer (50 mM Tris [pH 8.0], 0.5% SDS, 10 mM EDTA) and lysed for 10 min on ice. Lysates were sonicated in a Bioruptor sonicator (Diagenode) for 6 cycles of 30 s on/off for optimal shearing. Debris was pelleted, and chromatin-containing supernatants were diluted with 9 volumes of dilution buffer (0.005% SDS, 0.1% Triton X-100, 1.2 mM EDTA, 1.67 mM Tris [pH 8.0], 167 mM NaCl) and immunoprecipitated with E2F-2 antibody or rabbit IgG (Santa Cruz) overnight. Sheep anti-rabbit Dynabeads (Life Technologies) were washed and precleared overnight with PBS containing 0.5% BSA. Precleared beads were added to the immunoprecipitated lysates and left for 4 h. Beads were washed with shearing buffer, low-salt wash buffer (0.1% SDS, 1% Triton X-100, 2 mM EDTA, 20 mM Tris [pH 8.0], 150 mM NaCl), LiCl wash buffer (250 mM LiCl, 0.5% NP-40, 0.5% sodium deoxycholate, 1 mM EDTA, 10 mM Tris [pH 8.0]), and TE (10 mM Tris [pH 8.0], 1 mM EDTA) and magnetically isolated. Beads were resuspended in SDS elution buffer (1% SDS, 10 mM EDTA, 50 mM Tris [pH 8.0]) and incubated at 65°C overnight to reverse cross-links and elute proteins. Next, samples were treated with RNase A and 20 mg/ml proteinase K, and DNA was isolated. Quantitative real-time PCR was performed on a QuantStudio 6 instrument (Life Technologies) using SYBR green (Life Technologies). Oligonucleotide sequences are available upon request. Data are expressed as fold enrichment of E2F-2 pulldown over IgG relative to input controls.

Statistical analysis. All statistical analysis was performed using Prism (GraphPad). *P* values were calculated using Student's unpaired *t* test, except in the cases of nuclear area and nuclear polarity. For these calculations, data did not follow a normal distribution; thus, the Mann-Whitney test was used to calculate significance.

Accession number. RNA sequencing data are accessible at NCBI Gene Expression Omnibus under accession number GSE87127.

SUPPLEMENTAL MATERIAL

Supplemental material for this article may be found at https://doi.org/10.1128/MCB.00274-16.

TEXT S1, XLSX file, 0.01 MB.

ACKNOWLEDGMENTS

Study funding was provided by NIH grants R01HL104070 (M.M.P.) and R01HL098608 (A.C.M.) and an American Cancer Society Research Scholar Award (A.C.M.).

We acknowledge technical support from the Blood Research Institute (BloodCenter of Wisconsin) Flow Cytometry and Cell Imaging core facilities and the Yale University

School of Medicine Flow Cytometry core facility. We thank Navdeep Chandel and Cara Gottardi (Northwestern University) for helpful advice.

REFERENCES

1. Pop R, Shearstone JR, Shen Q, Liu Y, Hallstrom K, Koulnis M, Gribnau J, Socolovsky M. 2010. A key commitment step in erythropoiesis is synchronized with the cell cycle clock through mutual inhibition between PU.1 and S-phase progression. PLoS Biol 8:e1000484. https://doi.org/10.1371/journal.pbio.1000484.
2. Hsieh FF, Barnett LA, Green WF, Freedman K, Matushansky I, Skoultchi AI, Kelley LL. 2000. Cell cycle exit during terminal erythroid differentiation is associated with accumulation of p27(Kip1) and inactivation of cdk2 kinase. Blood 96:2746–2754.
3. Siatecka M, Lohmann F, Bao S, Bieker JJ. 2010. EKLF directly activates the p21WAF1/CIP1 gene by proximal promoter and novel intronic regulatory regions during erythroid differentiation. Mol Cell Biol 30:2811–2822. https://doi.org/10.1128/MCB.01016-09.
4. Gnanapragasam MN, McGrath KE, Catherman S, Xue L, Palis J, Bieker JJ. 2016. EKLF/KLF1-regulated cell cycle exit is essential for erythroblast enucleation. Blood 128:1631–1641. https://doi.org/10.1182/blood-2016-03-706671.
5. Sankaran VG, Orkin SH, Walkley CR. 2008. Rb intrinsically promotes erythropoiesis by coupling cell cycle exit with mitochondrial biogenesis. Genes Dev 22:463–475. https://doi.org/10.1101/gad.1627208.
6. Spike BT, Dirlam A, Dibling BC, Marvin J, Williams BO, Jacks T, Macleod KF. 2004. The Rb tumor suppressor is required for stress erythropoiesis. EMBO J 23:4319–4329. https://doi.org/10.1038/sj.emboj.7600432.
7. Ghazaryan S, Sy C, Hu T, An X, Mohandas N, Fu H, Aladjem MI, Chang VT, Opavsky R, Wu L. 2014. Inactivation of Rb and E2f8 synergizes to trigger stressed DNA replication during erythroid terminal differentiation. Mol Cell Biol 34:2833–2847. https://doi.org/10.1128/MCB.01651-13.
8. Dirlam A, Spike BT, Macleod KF. 2007. Deregulated E2f-2 underlies cell cycle and maturation defects in retinoblastoma null erythroblasts. Mol Cell Biol 27:8713–8728. https://doi.org/10.1128/MCB.01118-07.
9. Narasimha AM, Kaulich M, Shapiro GS, Choi YJ, Sicinski P, Dowdy SF. 2014. Cyclin D activates the Rb tumor suppressor by mono-phosphorylation. eLife 3:e02872.
10. Wander SA, Zhao D, Slingerland JM. 2011. p27: a barometer of signaling deregulation and potential predictor of response to targeted therapies. Clin Cancer Res 17:12–18. https://doi.org/10.1158/1078-0432.CCR-10-0752.
11. Sherr CJ, Roberts JM. 2004. Living with or without cyclins and cyclin-dependent kinases. Genes Dev 18:2699–2711. https://doi.org/10.1101/gad.1256504.
12. Minella AC, Loeb KR, Knecht A, Welcker M, Varnum-Finney BJ, Bernstein ID, Roberts JM, Clurman BE. 2008. Cyclin E phosphorylation regulates cell proliferation in hematopoietic and epithelial lineages in vivo. Genes Dev 22:1677–1689. https://doi.org/10.1101/gad.1650208.
13. Xu Y, Swartz KL, Siu KT, Bhattacharyya M, Minella AC. 2014. Fbw7-dependent cyclin E regulation ensures terminal maturation of bone marrow erythroid cells by restraining oxidative metabolism. Oncogene 33:3161–3171. https://doi.org/10.1038/onc.2013.289.
14. Siu KT, Xu Y, Swartz KL, Bhattacharyya M, Gurbuxani S, Hua Y, Minella AC. 2014. Chromosome instability underlies hematopoietic stem cell dysfunction and lymphoid neoplasia associated with impaired Fbw7-mediated cyclin E regulation. Mol Cell Biol 34:3244–3258. https://doi.org/10.1128/MCB.01528-13.
15. Li FX, Zhu JW, Hogan CJ, DeGregori J. 2003. Defective gene expression, S phase progression, and maturation during hematopoiesis in E2F1/E2F2 mutant mice. Mol Cell Biol 23:3607–3622. https://doi.org/10.1128/MCB.23.10.3607-3622.2003.
16. Pilon AM, Arcasoy MO, Dressman HK, Vayda SE, Maksimova YD, Sangerman JI, Gallagher PG, Bodine DM. 2008. Failure of terminal erythroid differentiation in EKLF-deficient mice is associated with cell cycle perturbation and reduced expression of E2F2. Mol Cell Biol 28:7394–7401. https://doi.org/10.1128/MCB.01087-08.
17. Tallack MR, Keys JR, Humbert PO, Perkins AC. 2009. EKLF/KLF1 controls cell cycle entry via direct regulation of E2f2. J Biol Chem 284:20966–20974. https://doi.org/10.1074/jbc.M109.006346.
18. Chen C, Lodish HF. 2014. Global analysis of induced transcription factors and cofactors identifies Tfdp2 as an essential coregulator during terminal erythropoiesis. Exp Hematol 42:464–476. https://doi.org/10.1016/j.exphem.2014.03.001.
19. Humbert PO, Rogers C, Ganiatsas S, Landsberg RL, Trimarchi JM, Dandapani S, Brugnara C, Erdman S, Schrenzel M, Bronson RT, Lees Jacqueline A. 2000. E2F4 is essential for normal erythrocyte maturation and neonatal viability. Mol Cell 6:281–291. https://doi.org/10.1016/S1097-2765(00)00029-0.
20. Kinross KM, Clark AJ, Iazzolino RM, Humbert PO. 2006. E2f4 regulates fetal erythropoiesis through the promotion of cellular proliferation. Blood 108:886–895. https://doi.org/10.1182/blood-2005-09-008656.
21. Kingsley PD, Greenfest-Allen E, Frame JM, Bushnell TP, Malik J, McGrath KE, Stoeckert CJ, Palis J. 2013. Ontogeny of erythroid gene expression. Blood 121:e5–e13. https://doi.org/10.1182/blood-2012-04-422394.
22. Chen K, Liu J, Heck S, Chasis JA, An X, Mohandas N. 2009. Resolving the distinct stages in erythroid differentiation based on dynamic changes in membrane protein expression during erythropoiesis. Proc Natl Acad Sci U S A 106:17413–17418. https://doi.org/10.1073/pnas.0909296106.
23. Zhang J, Socolovsky M, Gross AW, Lodish HF. 2003. Role of Ras signaling in erythroid differentiation of mouse fetal liver cells: functional analysis by a flow cytometry-based novel culture system. Blood 102:3938–3946. https://doi.org/10.1182/blood-2003-05-1479.
24. Trimarchi JM, Lees JA. 2002. Sibling rivalry in the E2F family. Nat Rev Mol Cell Biol 3:11–20.
25. Dimova DK, Dyson NJ. 2005. The E2F transcriptional network: old acquaintances with new faces. Oncogene 24:2810–2826. https://doi.org/10.1038/sj.onc.1208612.
26. Geng Y, Eaton EN, Picón M, Roberts JM, Lundberg AS, Gifford A, Sardet C, Weinberg RA. 1996. Regulation of cyclin E transcription by E2Fs and retinoblastoma protein. Oncogene 12:1173–1180.
27. Paulson RF, Shi L, Wu D-C. 2011. Stress erythropoiesis: new signals and new stress progenitor cells. Curr Opin Hematol 18:139–145. https://doi.org/10.1097/MOH.0b013e32834521c8.
28. Socolovsky M. 2007. Molecular insights into stress erythropoiesis. Curr Opin Hematol 14:215–224. https://doi.org/10.1097/MOH.0b013e3280de2bf1.
29. Begg AC, McNally NJ, Shrieve DC, Kärcher H. 1985. A method to measure the duration of DNA synthesis and the potential doubling time from a single sample. Cytometry 6:620–626. https://doi.org/10.1002/cyto.990060618.
30. Huang DW, Sherman BT, Lempicki RA. 2009. Systematic and integrative analysis of large gene lists using DAVID bioinformatics resources. Nat Protoc 4:44–57. https://doi.org/10.1038/nprot.2008.211.
31. Ji P, Jayapal SR, Lodish HF. 2008. Enucleation of cultured mouse fetal erythroblasts requires Rac GTPases and mDia2. Nat Cell Biol 10:314–321. https://doi.org/10.1038/ncb1693.
32. Bassi ZI, Verbrugghe KJ, Capalbo L, Gregory S, Montembault E, Glover DM, D'Avino PP. 2011. Sticky/Citron kinase maintains proper RhoA localization at the cleavage site during cytokinesis. J Cell Biol 195:595–603. https://doi.org/10.1083/jcb.201105136.
33. Gai M, Camera P, Dema A, Bianchi F, Berto G, Scarpa E, Germena G, Di Cunto F. 2011. Citron kinase controls abscission through RhoA and anillin. Mol Biol Cell 22:3768–3778. https://doi.org/10.1091/mbc.E10-12-0952.
34. Gruneberg U, Neef R, Li X, Chan EHY, Chalamalasetty RB, Nigg EA, Barr FA. 2006. KIF14 and citron kinase act together to promote efficient cytokinesis. J Cell Biol 172:363–372. https://doi.org/10.1083/jcb.200511061.
35. Eda M, Yonemura S, Kato T, Watanabe N, Ishizaki T, Madaule P, Narumiya S. 2001. Rho-dependent transfer of Citron-kinase to the cleavage furrow of dividing cells. J Cell Sci 114:3273–3284.
36. Gai M, Bianchi FT, Vagnoni C, Vernì F, Bonaccorsi S, Pasquero S, Berto GE, Sgrò F, Chiotto AM, Annaratone L, Sapino A, Bergo A, Landsberger N, Bond J, Huttner WB, Di Cunto F. 2016. ASPM and CITK regulate spindle orientation by affecting the dynamics of astral microtubules. EMBO Rep 17:1396–1409. https://doi.org/10.15252/embr.201541823.
37. Konstantinidis DG, Pushkaran S, Johnson JF, Cancelas JA, Manganaris S, Harris CE, Williams DA, Zheng Y, Kalfa TA. 2012. Signaling and cytoskel-

etal requirements in erythroblast enucleation. Blood 119:6118–6127. https://doi.org/10.1182/blood-2011-09-379263.
38. Welch JJ, Watts JA, Vakoc CR, Yao Y, Wang H, Hardison RC, Blobel GA, Chodosh LA, Weiss MJ. 2004. Global regulation of erythroid gene expression by transcription factor GATA-1. Blood 104:3136–3147. https://doi.org/10.1182/blood-2004-04-1603.
39. Weiss MJ, Yu C, Orkin SH. 1997. Erythroid-cell-specific properties of transcription factor GATA-1 revealed by phenotypic rescue of a gene-targeted cell line. Mol Cell Biol 17:1642–1651. https://doi.org/10.1128/MCB.17.3.1642.
40. Pishesha N, Thiru P, Shi J, Eng Sankaran JCVG, Lodish HF. 2014. Transcriptional divergence and conservation of human and mouse erythropoiesis. Proc Natl Acad Sci U S A 111:4103–4108. https://doi.org/10.1073/pnas.1401598111.
41. Yamashiro S, Totsukawa G, Yamakita Y, Sasaki Y, Madaule P, Ishizaki T, Narumiya S, Matsumura F. 2003. Citron kinase, a Rho-dependent kinase, induces di-phosphorylation of regulatory light chain of myosin II. Mol Biol Cell 14:1745–1756. https://doi.org/10.1091/mbc.E02-07-0427.
42. Davis MI, Hunt JP, Herrgard S, Ciceri P, Wodicka LM, Pallares G, Hocker M, Treiber DK, Zarrinkar PP. 2011. Comprehensive analysis of kinase inhibitor selectivity. Nat Biotechnol 29:1046–1051. https://doi.org/10.1038/nbt.1990.
43. Yan L. 2009. MK-2206: a potent oral allosteric AKT inhibitor, abstr DDT01-1. Proc Am Assoc Cancer Res, Denver, CO, 1 to 22 April 2009.
44. Hirai H, Sootome H, Nakatsuru Y, Miyama K, Taguchi S, Tsujioka K, Ueno Y, Hatch H, Majumder PK, Pan B-S, Kotani H. 2010. MK-2206, an allosteric Akt inhibitor, enhances antitumor efficacy by standard chemotherapeutic agents or molecular targeted drugs in vitro and in vivo. Mol Cancer Ther 9:1956–1967. https://doi.org/10.1158/1535-7163.MCT-09-1012.
45. Kingsley PD, Malik J, Fantauzzo KA, Palis J. 2004. Yolk sac-derived primitive erythroblasts enucleate during mammalian embryogenesis. Blood 104:19–25. https://doi.org/10.1182/blood-2003-12-4162.
46. Zhao B, Mei Y, Schipma MJ, Roth EW, Bleher R, Rappoport JZ, Wickrema A, Yang J, Ji P. 2016. Nuclear condensation during mouse erythropoiesis requires caspase-3-mediated nuclear opening. Dev Cell 36:498–510. https://doi.org/10.1016/j.devcel.2016.02.001.
47. Thom CS, Traxler EA, Khandros E, Nickas JM, Zhou OY, Lazarus JE, Silva APG, Prabhu D, Yao Y, Aribeana C, Fuchs SY, Mackay JP, Holzbaur ELF, Weiss MJ. 2014. Trim58 degrades dynein and regulates terminal erythropoiesis. Dev Cell 30:688–700. https://doi.org/10.1016/j.devcel.2014.07.021.
48. Keerthivasan G, Small S, Liu H, Wickrema A, Crispino JD. 2010. Vesicle trafficking plays a novel role in erythroblast enucleation. Blood 116:3331–3340. https://doi.org/10.1182/blood-2010-03-277426.
49. Maliga Z, Junqueira M, Toyoda Y, Ettinger A, Mora-Bermúdez F, Klemm RW, Vasilj A, Guhr E, Ibarlucea-Benitez I, Poser I, Bonifacio E, Huttner WB, Shevchenko A, Hyman AA. 2013. A genomic toolkit to investigate kinesin and myosin motor function in cells. Nat Cell Biol 15:325–334. https://doi.org/10.1038/ncb2689.
50. Schindelin J, Arganda-Carreras I, Frise E, Kaynig V, Longair M, Pietzsch T, Preibisch S, Rueden C, Saalfeld S, Schmid B, Tinevez J-Y, White DJ, Hartenstein V, Eliceiri K, Tomancak P, Cardona A. 2012. Fiji: an open-source platform for biological-image analysis. Nat Methods 9:676–682. https://doi.org/10.1038/nmeth.2019.
51. Huang L-K, Wang M-JJ. 1995. Image thresholding by minimizing the measures of fuzziness. Pattern Recognit 28:41–51. https://doi.org/10.1016/0031-3203(94)E0043-K.
52. Soille P, Vincent LM. 1990. Determining watersheds in digital pictures via flooding simulations, p 240–250. *In* Kunt M (ed), Visual communications and image processing '90. SPIE, Bellingham, WA.